Journal of The Electrochemical Society, **152** (1) H6-H11 (2005)
0013-4651/2004/152(1)/H6/6/$7.00 © The Electrochemical Society, Inc.

Design and Testing of an Impedance-Based Sensor for Monitoring Drug Delivery

Audrey M. Johnson,[a] Donald R. Sadoway,[b,*] Michael J. Cima,[b] and Robert Langer[a,z]

[a]*Department of Chemical Engineering and* [b]*Department of Materials Science and Engineering, Massachusetts Institute of Technology, Cambridge, Massachusetts 02139, USA*

A new impedance-based sensor to monitor drug delivery from an implantable microelectromechanical systems (MEMS) device has been fabricated and tested. The sensor consists of two electrodes on opposing sides of a pyramidal drug reservoir. The dissolution of the drug and advance of solution into the reservoir cause the impedance to change over time. A 100 times scale model of the sensor was constructed to examine the effects of electrode geometry on solution resistance. An equivalent circuit was formulated to interpret the impedance signal in terms of the resistance and double-layer capacitance of the solution in the reservoir. The circuit was validated by impedance measurements on reservoirs filled with phosphate-buffered saline solutions of varying concentrations. The sensor was then used to monitor the dissolution of the model drug mannitol from the drug delivery MEMS device. The measured solution resistance and double-layer capacitance are related to the rate of transport of drug from the device, making this sensor a potential instrument for noninvasive monitoring of drug transport from the implant *in vivo*. Experimental results agree closely with the expected values of capacitance, resistance, and dissolution time calculated from physical parameters.
 [DOI: 10.1149/1.1824045]

Manuscript submitted January 26, 2004; revised manuscript received June 11, 2004. Available electronically November 22, 2004.

A sensor for characterizing the transport of a drug from an implant *in vivo*, in real time and noninvasively, would have the potential to yield new information about the body's response to implants and the impact on drug or analyte transport. Understanding *in vivo* transport is critical for a number of applications including active drug delivery devices and long-term implantable sensors. Most current methods for measuring drug transport from implants are invasive and destructive.[1-4] We have designed and tested a novel sensor that allows the monitoring of drug dissolution from an implantable microelectromechanical systems (MEMS) device in real time without disturbing the medium through which the drug is diffusing. Furthermore, the physical disposition of the sensor is such that without recalibration it can continue to give meaningful data even under changing conditions in the surrounding tissue, *e.g.*, implant encapsulation.

Implants are often walled off from the rest of the body by an avascular fibrous capsule of tissue that inhibits transport of substances such as oxygen or nutrients between the body and the implant.[5] The formation of a fibrous capsule around implanted devices has particularly important implications for drug delivery and sensing applications. Current drug delivery implants are usually designed for a slow, steady release of a drug over time. In such a case, the transport profile of drug is pseudo-steady state, so that while the fibrous capsule affects drug release, the device is still able to function.[6,7] However, in the case of active devices, where quick pulsatile or more complex release profiles are desired, the isolation of the implant causes a time lag due to the finite amount of time required for diffusion of the drug through the capsule.[8,9] This time delay is also a key factor in the performance of *in vivo* sensors.[10,11] Even if sensor components are made resistant to the immune response, the sensor must be continually recalibrated to account for the changing conditions in the tissue surrounding it.[12]

Most methods for determining the extent of implant encapsulation and the drug dissolution profile in the vicinity of an implant involve invasive methods that result in the destruction of the sample. Each data point requires a different implant and animal, contributing to a high variability in measurements. Nondestructive methods have significant limitations. Those involving direct observation of drug are restricted to unique systems such as the translucent rabbit ear[13] or rat dorsal skin clamped in a glass window for viewing.[14] Pharmacokinetic studies also involve monitoring of drug distributions *in vivo* through such methods as microdialysis[15,16] and nuclear imaging;[17,18] however these techniques are limited in their resolution, accuracy, and/or detection limits.[19-21] Measurements of blood and urine drug levels also give some feedback on the operation of a drug delivery device. However, many transport barriers exist between the implant region and the point of measurement, and the complex pharmacokinetics of many drugs further complicates the interpretation of these measurements.[22-24]

A drug delivery MEMS device has been developed previously in our laboratory which allows the release of multiple drugs in a pulsatile fashion.[25,26] It consists of an array of microreservoirs etched into a silicon substrate, each capped by a thin gold membrane. Upon application of a 1 V potential in the presence of chloride ion, the gold membrane oxidizes to form soluble gold chloride, thinning the membrane until it fails. The drug within the reservoir then dissolves into the surroundings as the aqueous solution advances into the reservoir.

This paper presents a modification of the drug delivery MEMS device in which two electrodes within each drug reservoir serve as a novel drug release sensor, as depicted in Fig. 1. Each reservoir has the shape of a square pyramid due to the anisotropic etch used to create them, and the electrodes cover two opposing sides of this pyramid. Two-electrode impedance spectroscopy is used to measure the electrical characteristics of the reservoir. As the drug dissolves, the change in the electrical signature of the system allows real time monitoring of the rate of transport of drug away from the device. The utility of the sensor was demonstrated by *in vitro* measurements interpreted by means of an equivalent circuit.

Experimental

Chemicals.—D-mannitol and potassium chloride (Sigma, St. Louis, MO) were used as received. Phosphate buffered saline, PBS, consisting of 0.137 M NaCl, 0.001 M KH_2PO_4, 0.01 M Na_2HPO_4, and 0.0027 M KCl at pH 7.4 when diluted to 1 time concentration (Roche, Indianapolis, IN) was purchased as a 10 times solution and diluted to the appropriate concentration. Solutions were made with deionized water passed through a MilliQ (Millipore, Billerica, MA) system, resistivity above 17.8 MΩ cm. Wires and bond pads were insulated with EP42HT medical grade epoxy (MasterBond, Hackensack, NJ), cured for 24 h at room temperature.

Microfabrication of devices.—Drug delivery MEMS devices were fabricated in the Microsystems Technology Laboratory at MIT. Silicon wafers were 4 in., double-side polished, 300 μm thick, 1-10 Ω cm, p-doped ⟨100⟩ silicon (WaferNet, San Jose, CA). A 100 nm thermal oxide layer was grown on both surfaces and covered with a 150 nm low pressure chemical vapor deposition (LPCVD) nitride

* Electrochemical Society Active Member.
z E-mail: rlanger@mit.edu

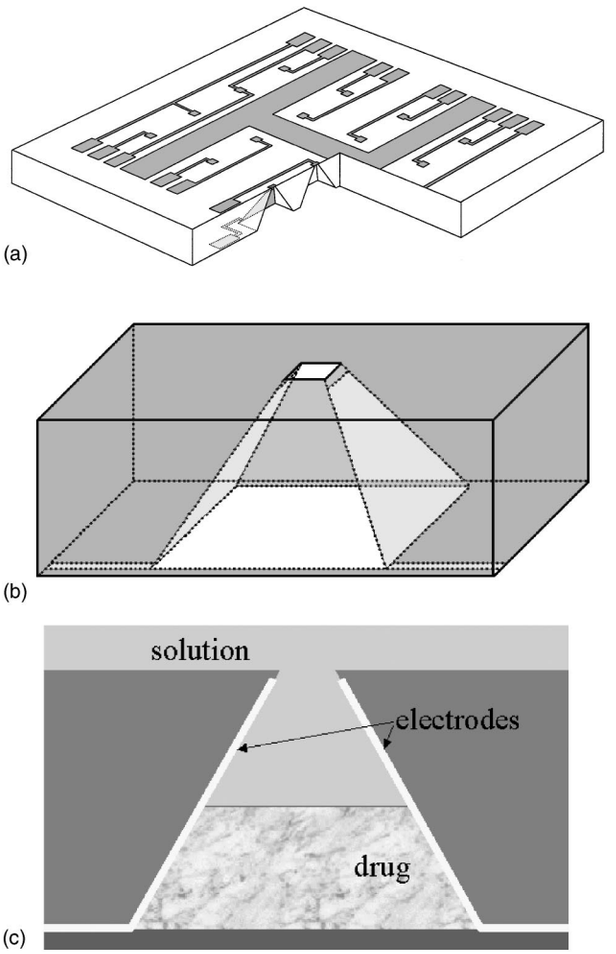

Figure 1. The drug delivery MEMS device: (a) cutaway perspective view of the prototype, with electrodes on the top surface for drug release and electrodes on the bottom surface and in the reservoirs for drug release monitoring, dimensions 5 × 5 × 0.3 mm; (b) view of one device reservoir showing electrode configuration to scale; (c) idealized representation of drug release from a reservoir.

layer to act as an etch stop (standard batch diffusion furnaces, Thermco 10K, La Porte, IN). The back sides of the wafers were patterned with an array of 480 μm squares using positive photoresist (OCG825-20, Arch Chemicals, Norwalk, CT), which were plasma etched through the nitride and oxide layers (Plasmaquest Series II Reactor model 145, MKS Instruments, Andover, MA). Wafers were immersed in 5.17 M potassium hydroxide at 85°C until the silicon had been etched through the entire thickness of the wafers to form an array of pyramidal reservoirs capped by nitride/oxide membranes. The front sides of the wafers were then patterned with electrodes for the triggering of drug release from reservoirs using image-reversal resist (AZ5214 E, Clariant, Somerville, NJ). Electron beam evaporation (model VES 2550, Temescal Semiconductor Products, Fairfield, CA) was used to deposit 300 nm gold sandwiched between two 10 nm titanium adhesion layers, and the image-reversal resist pattern was lifted off in acetone. The remaining nitride and oxide were removed from the back sides of the wafers by plasma etching, and a conformal 100 nm oxide layer was deposited by plasma deposition at 80°C (Plasmaquest Series II, model 145). A shadow mask wafer[27] was prepared separately by deep reactive ion etching (DRIE) etching a wafer with the pattern of the gold impedance electrodes to be deposited inside the device reservoirs (DRIE Multiplex ICP, Surface Technology Systems, Portsmouth, NH). The shadow mask was aligned over the device wafer (Karl Suss MA4 Aligner, Suss MicroTec Inc., Waterbury Center, VT) and 300 nm gold over a 10 nm titanium adhesion layer was deposited via electron beam evaporation to form the impedance electrodes. A 650 nm thick oxide layer was deposited by plasma deposition and patterned over the front sides of the wafers to insulate the trigger electrodes from the environment. Wafers were then diced into 5 × 5 mm devices on an automatic dicing saw (2060 blade, DAD-2H/6T dicing saw, Disco Hi-Tec America, Inc., Santa Clara, CA).

Scale model of device reservoirs.—A 100 times scale model of a square pyramidal drug delivery device reservoir was fabricated from acrylic by the MIT machine shop. The pyramid was of base length 4.8 cm, height 3.0 cm, and base angle 54.4°. One side of the pyramid was removable to provide access to the pyramid interior. Gold foil electrodes (25 μm thick, 99.9^{+}%, Sigma) were cut to cover two opposing interior sides of the pyramid with tabs extending from the top of the model for electrical connections.

PBS solution conductivity measurements.—The conductivities of PBS solutions were measured using a two-electrode conductivity cell (Industrial Instruments, Inc., Cedar Grove, NJ) fully immersed in the solution to be measured. The impedance spectrum was recorded using a Solartron 1255B frequency response analyzer with a SI1287 electrochemical interface. The impedance was measured for frequencies between 10^2 and 10^6 Hz, sufficient to reveal the critical point or notch in the Cole-Cole plot. The critical point was independent of the magnitude of the ac excitation voltage. The cell constant was determined using standard solutions of 0.01 D,[c] 0.1 D, and 1.0 D potassium chloride. All solutions were kept at room temperature, 23.5°C, and the conductivities of the standard solutions at this temperature were interpolated from values given by Wu and Koch.[28] The measured value of the cell constant was then used to determine the conductivity of 0.01, 0.1, 0.5, and 1.0 times PBS solutions.

Impedance of reservoir scale model.—The two-electrode impedance of the 100 times scale model of a device reservoir was measured for frequencies between 10 and 10^6 Hz. An initial aliquot of 1.0 times PBS was added to the model to make contact between the foil electrodes and the impedance measurement was repeated. The impedance measurement and addition of PBS was repeated in increments of 1 to 2 mL solution until the model was entirely full. The experiment was repeated using 0.5 times PBS and 0.1 times PBS solutions.

Impedance of microdevice reservoirs.—A drug delivery MEMS device was packaged with open reservoirs for measurement of impedance submersed in PBS solutions. The impedance electrodes were connected by traces to bond pads along the edges of the device. Insulated gold wires were epoxied (MasterBond EP42HT) alongside the device and gold wire bonds, diameter 25 μm, were made between the bond pads and the wires. The wires, bonds, pads, and traces were covered with epoxy to insulate them. The two-electrode impedance of each of four reservoirs was measured for frequencies between 10 and 10^6 Hz. The device was then submersed in PBS solutions of 1.0, 0.5, and 0.1 times concentration. The solutions were observed to entirely fill the reservoirs, and the impedance measurement across each reservoir was repeated in each solution.

Impedance during drug release.—The reservoirs of a drug delivery MEMS device were completely filled with 35-45 μg solid mannitol per reservoir by a melt process. First, powdered mannitol was spread over the reservoirs of a template device and heated, melting it into the reservoirs. Excess mannitol was removed with a razor blade, and the pyramid-shaped mannitol pieces remaining were removed from the reservoirs. These presized mannitol pieces were then placed into the reservoirs of the drug delivery MEMS device, heated to melt them in place, and weighed (AD-4 Autobalance,

[c] The demal (D) is a concentration unit used in connection with the electrical conductivity of aqueous solutions.[28]

Table I. Conductivity of PBS solutions.

PBS concentration (times)	Calculated conductivity at 25°C (S cm^{-1})	Measured conductivity at 23.5°C (S cm^{-1})
1.0	1.59×10^{-2}	1.57×10^{-2}
0.5	8.37×10^{-3}	8.32×10^{-3}
0.1	1.81×10^{-3}	1.79×10^{-3}
0.01	1.90×10^{-4}	1.88×10^{-4}

Perkin-Elmer, Boston, MA). The device reservoirs were then sealed with a small piece of a glass coverslip and epoxy, and gold wires were epoxied beside the bond pads. Wire bonds were made between the impedance electrodes of each reservoir and the wires, then insulated with epoxy. The two-electrode impedance of each reservoir was measured at frequencies between 10^3 and 10^6 Hz. The device was then submersed in 1.0 times PBS solution, and the impedance measurement was repeated. After each reservoir was opened, the reservoir impedance was measured every 3 min until the impedance did not change with time. At this point it was assumed that the dissolution of the mannitol was complete.

Results and Discussion

PBS solution conductivity.—The measured values of the electrical conductivity of solutions of 1.0, 0.5, 0.1, and 0.01 times PBS at room temperature, 23.5°C, are given in Table I. For comparison, the expected conductivity at 25°C was estimated by summing the molar conductivities of the ionic species present in each PBS solution. Molar conductivities of ionic species were interpolated from reported values (KCl, NaCl, except for 1.0 times PBS, which was extrapolated from the nearest reported value) or extrapolated from the limiting molar conductivity (Na_2HPO_4, KH_2PO_4) using Kohlrausch's law.[29,30] Standard KCl solutions gave a value of 1.00 $\pm$ 0.01 cm^{-1} for the cell constant.

Impedance of 100 times scale model.—The scale model of the pyramidal reservoir was constructed to evaluate the effects of the unusual electrode geometry on the impedance. The expected equivalent circuit and impedance for the system, an aqueous solution with no Faradaic processes occurring,[31] is shown in Fig. 2. The Cole-Cole plot for such a system is a vertical line with a real intercept equal to the solution resistance. In physical systems it is generally observed that a constant phase element (CPE) fits the data better than a simple capacitor. This is also true in our case, as the Cole-Cole plot has a finite, positive slope. However, although it is generally assumed that some sort of dispersion of physical properties gives rise to CPE behavior, the physics behind this are not well understood,[32] and we found it unnecessary to resort to the inclusion of a CPE in order to obtain a reasonably good fit to the data.

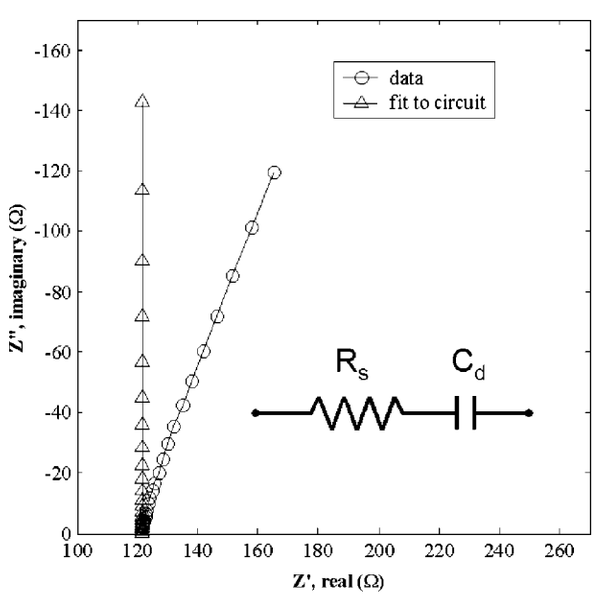

Figure 2. Equivalent circuit and Cole-Cole plot of experimental data and best fit to circuit for 100 times scale model of a square pyramidal drug reservoir containing 10 mL of 1.0 times PBS.

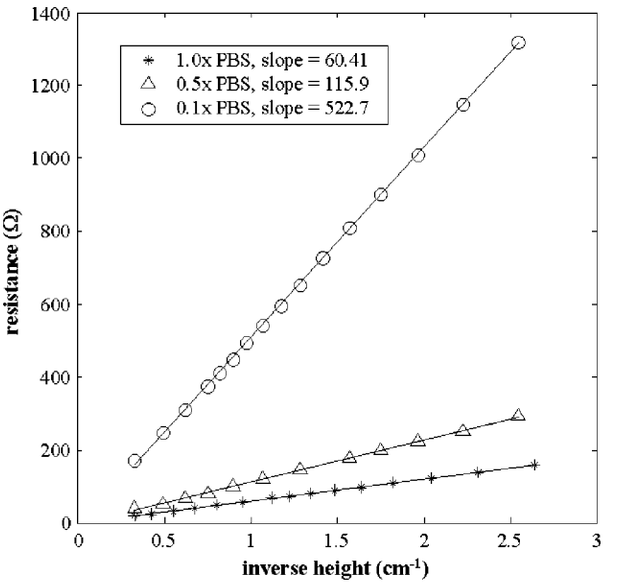

Figure 3. The dependence of the measured solution resistance in the square pyramidal model on height of the solution in the model and PBS concentration.

The resistance of a square pyramid can be calculated by starting with the formula for conductance of a solid

$$Y = A/\rho L$$

where A is the cross-sectional area, ρ is the resistivity, and L is the length. By taking a differential horizontal cross section, we can integrate the conductivities of each slice from $x = 0$ to $x = H$, where H is the height of the pyramid. In this case, A and L are both functions of x and of the base angle of the pyramid. For a square pyramid, at any height, x, the width of the electrode at the edge and the distance between the electrodes are the same function of x, $L(x)$. This means that the differential area is given by

$$dA = L(x)dx$$

Substituting into the equation for Y gives the formula

$$dY = L(x)dx/\rho L(x)$$

The $L(x)$ cancel out, and the equation is easily integrated from zero to H, yielding

$$Y = H/\rho, \quad R = \rho/H$$

From this formula we see that for the special case of a square pyramid, the resistance scales with the inverse of the height of the pyramid. Therefore, as the pyramid model is filled with solution, the resistance should scale with the inverse of the height of liquid in the model. This matches the experimental findings as shown in Fig. 3. In an ideal case the slope of the plot should be equal to the solution resistivity, which is the inverse of the conductivity measurements in Table I. For our system the linear least squares slope for each solu-

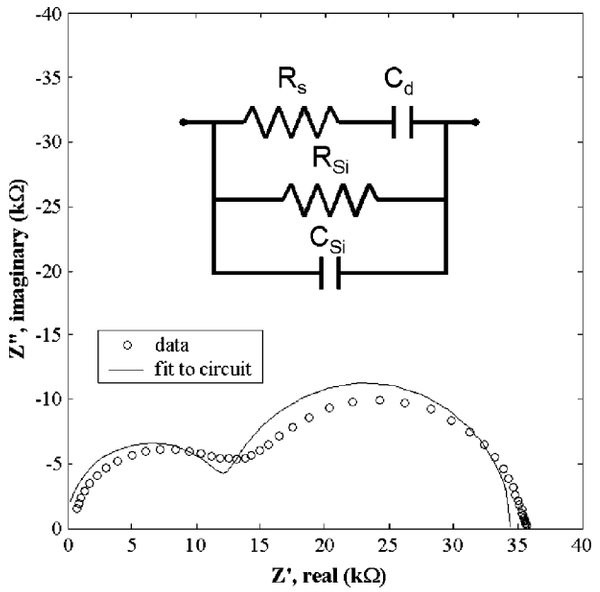

Figure 4. Equivalent circuit and Cole-Cole plot of experimental data and best fit to circuit for a drug delivery MEMS device reservoir filled with 0.1 times PBS. Similar results were obtained for solutions of higher ionic strength and for different device reservoirs.

tion differs from the resistivity by a factor of 0.95 ± 0.01, which gives us an effective cell constant for this particular experimental setup of $0.95/H$, very close to the theoretical cell constant of $1/H$ derived above. The experimental data agree very well with the predicted equivalent circuit and expected values for solution resistance. In addition, the double-layer capacitance for an aqueous solution is expected to be on the order of 10 $\mu F/cm^2$, and the best fit capacitance for our data agrees with this estimate.

Impedance of drug delivery MEMS reservoirs.—The resistance of a square pyramid calculated above was then compared to the resistance measured in the drug delivery device reservoir. For the microsystem the equivalent circuit is not as simple, as shown in Fig. 4. The parallel resistance and capacitance arise from a parallel current path through the silicon substrate in which the reservoir is etched. This path is due to leakage current from the electrodes through the silicon oxide layer beneath into the silicon, and takes the form of a parallel RC circuit, a so-called leaky capacitor. The magnitude of the leak current is determined by the connection between the wire bonds and the bond pads. This varies from reservoir to reservoir due to the inconsistency of the wire bonding process. For any particular reservoir the resistance and capacitance of this path were found to be independent of reservoir contents, as expected. The resistance remained constant within 3% during all experiments and the capacitance was constant within 10%.

The Cole-Cole plot of this circuit is two overlapping semicircles, which corresponds well to the experimental data, as depicted in the representative data fit given in Fig. 4. The solution resistance depends on the ionic strength of the solution and determines the position of the inflection point between the semicircles, while the silicon resistance depends on the device reservoir and determines the overall width of the curve. Some depression of the data from the ideal fit was observed, but again, a reasonably good fit was obtained without the substitution of a CPE for the capacitive elements.

The average solution resistance and double-layer capacitance of the device reservoirs are given in Table II. The double-layer capacitance is of the correct order of magnitude, a factor of 10^4 smaller than that observed for the 100 times scale model. The measured solution resistance is lower than that calculated using the formula for the resistance of a square pyramid by a factor of 0.86 ± 0.02.

Table II. Solution resistance and double-layer capacitance of microreservoirs filled with PBS.

PBS concentration (times)	Predicted solution resistance (kΩ)	Measured solution resistance (kΩ)	Measured double layer capacitance (nF)
1.0	2.13	1.79 ± 0.12	3.54 ± 0.79
0.5	4.01	3.68 ± 0.44	2.50 ± 0.62
0.1	18.6	16.0 ± 4.7	1.9 ± 1.6

This is likely due to fringing at the edges of the electric field, which is more significant in smaller systems. Taken together, these observations demonstrate the validity of the equivalent circuit of Fig. 4, giving us a good understanding of the physical system.

Monitoring drug release by impedance measurements.—A goal of this work was to demonstrate that the measurement of impedance would allow us to monitor the rate of drug release from a MEMS device reservoir in real time. A typical example of the impedance measurement during release of mannitol, a model drug, from a device reservoir is shown in Fig. 5a and b, as a succession of Cole-Cole and Bode plots. The impedance before opening the reservoir is similar to that observed for reservoirs full of air, which is expected because mannitol is a semicrystalline solid with negligible conductivity, and there is no electrolyte present for conduction. After opening the reservoir, the impedance changes gradually from the single semicircle characteristic of the RC parallel circuit to the overlapping double semicircle characteristic of the circuit in Fig. 4. The solution resistance drops as the saline solution provides an ever larger low resistance path between the electrodes, and the double-layer capacitance increases as the area of the electrodes in contact with solution increases. Successive data fits to this circuit give the values of solution resistance and double-layer capacitance *vs.* time shown in Fig. 5c. This corresponds to the dissolution of the mannitol and the advance of the PBS solvent front into the reservoir. The dissolution is largely complete after 90 mins. Further experiments with radiolabeled mannitol indicate that the gradual change in sensor output parallels the rate of release measured by scintillation counting of the release medium.

For comparison, a first-order estimate of the expected time for dissolution can be made by considering the dissolution and diffusion of a solid in one dimension.[33,34] A mass balance gives the following equation for $C(x,t)$

$$\partial C/\partial t = D\partial^2 C/\partial x^2; \quad C(x,0) = 0$$

$$C(0,t) = C_{sat}; \quad C(\infty,t) = 0$$

where C_{sat} is the solubility of the compound in solution and D is the diffusivity. This can be solved for the flux at the interface as a function of time[35]

$$N_x|_{x=0} = -D \ dC/dx|_{x=0} = C_{sat}(D/\pi t)^{1/2}$$

A mass balance at the interface between solid and liquid can be written as

$$-AD \ dC/dx|_{x=0}dt = A(C_s - C_{sat})dz$$

where A is the area exposed to solution, C_s is the density of the solid compound, and dz is the differential distance traveled by the interface in the time dt. Note that the equation for $C(x,t)$ is only valid if we make the assumption that the motion of the interface is slow compared to the formation of the concentration profile (pseudosteady state). If we substitute the expression for the flux at the interface into the interfacial mass balance, we obtain an expression for the distance traveled by the interface (the depth of penetration of solvent into the reservoir) as a function of time

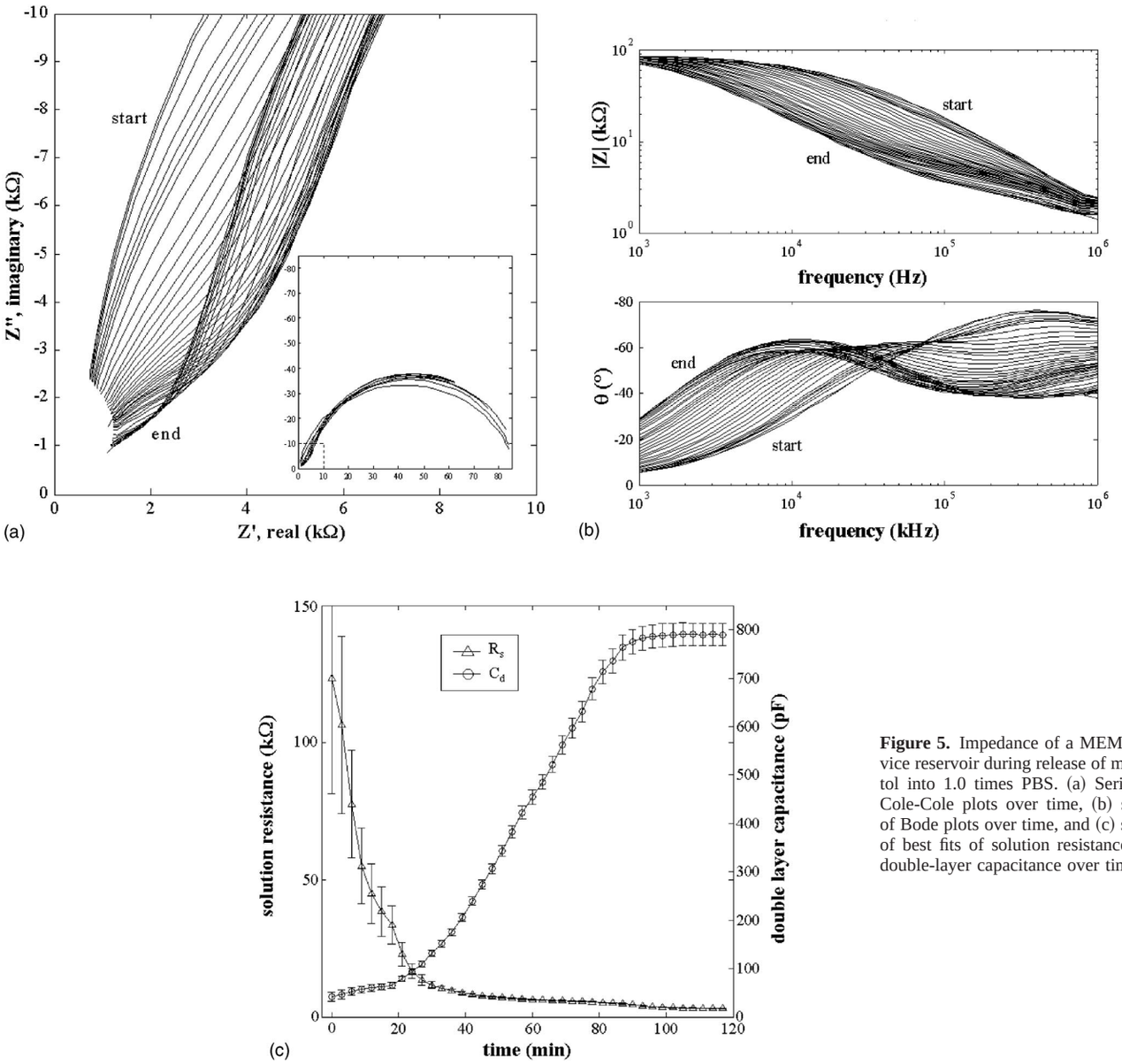

Figure 5. Impedance of a MEMS device reservoir during release of mannitol into 1.0 times PBS. (a) Series of Cole-Cole plots over time, (b) series of Bode plots over time, and (c) series of best fits of solution resistance and double-layer capacitance over time.

$$z(t) = 2[C_{sat}/(C_s - C_{sat})](Dt/\pi)^{1/2}$$

Substituting appropriate values for the physical parameters (C_{sat} = 0.18 g/cm^3, C_s = 1.5 g/cm^3, $D = 10^{-5}$ cm^2/s, z = 300 μm), we obtain an estimated time for dissolution of ~80 min, which agrees quite closely with the experimentally observed dissolution time.

The impedance-based sensor was used to monitor dissolution of mannitol *in vitro* and the relationship between sensor output and the physical system was characterized by an appropriate equivalent circuit. Future experiments will evaluate the relationship between the sensor output and the rate of transport of the drug through various transport barriers. In addition, it would be useful to compare sensor output to traditional methods of evaluating drug release, such as radio-label or fluorophore detection. Finally, a critical test will be to use the sensor to monitor drug release during long-term implantation *in vivo*, evaluating the impact of fibrous capsule development on drug transport. The nondestructive nature of the measurement will allow repeated measurements of drug release from the same implant at multiple time points, without the need for explantation or disruption of the tissue environment.

Conclusion

The drug delivery MEMS device with an impedance-based sensor successfully monitored the release of a drug from a device reservoir. The system was represented by a simple equivalent circuit whose elements correspond to the physical characteristics of the system. The solution resistance and double-layer capacitance were measured as functions of time during release of the drug. These two parameters are functions of the degree of penetration of solution into the reservoir during drug release, which can be related to the rate of transport of the drug from the device. The sensor has the potential to be used as a novel method for noninvasive monitoring of drug transport from the implant *in vivo*.

Acknowledgments

We thank Dr. D. DeLongchamp and Professor M. Zahn for discussions of equivalent circuit analysis, and Dr. R. Shawgo and Dr. L.

Arana for help with packaging and microfabrication aspects of the project. This work was supported by U.S. NIH grant no. 1 R24 AI47739-01 and graduate fellowships from the U.S. NSF and Merck.

Massachusetts Institute of Technology assisted in meeting the publication costs of this article.

References

1. J. F. Strasser, L. K. Fun, S. Eller, S. A. Grossman, and W. M. Saltzman, *J. Pharmacol. Exp. Ther.*, **275**, 1647 (1995).
2. P. Kortesuo, M. Ahola, S. Karlsson, I. Kangasniemi, A. Yli-Urpo, and J. Kiesvaara, *Biomaterials*, **21**, 193 (2000).
3. A. A. Sharkawy, B. Klitzman, G. A. Truskey, and W. M. Reichert, *J. Biomed. Mater. Res.*, **37**, 401 (1997).
4. R. C. Wood, E. L. LeCluyse, and J. A. Fix, *Biomaterials*, **16**, 957 (1995).
5. J. Bodziony, *Res. Exp. Med.*, **192**, 305 (1992).
6. B. D. Ratner, *J. Controlled Release*, **78**, 211 (2002).
7. J. M. Anderson, H. Niven, J. Pelagalli, L. S. Olanoff, and R. D. Jones, *J. Biomed. Mater. Res.*, **15**, 889 (1981).
8. P. S. Leppert, L. Cammack, R. Cargill, L. Coffman, M. Cortese, K. Engle, C. Krupco, and J. A. Fix, *J. Biomed. Mater. Res.*, **28**, 713 (1994).
9. E. Fournier, C. Passirani, C. N. Montero-Menei, and J. P. Benoit, *Biomaterials*, **24**, 3311 (2003).
10. M. C. Frost and M. E. Meyerhoff, *Curr. Opin. Chem. Biol.*, **6**, 633 (2002).
11. M. Gerritsen, J. A. Jansen, A. Kros, R. J. M. Nolte, and J. A. Lutterman, *J. Invest. Surg.*, **11**, 163 (1998).
12. C. Choleau, J. C. Klein, G. Reach, B. Aussedat, V. Demaria-Pesce, G. S. Wilson, R. Gifford, and W. K. Ward, *Biosens. Bioelectron.*, **17**, 647 (2002).
13. G. R. Martin and R. K. Jain, *Cancer Res.*, **54**, 5670 (1994).
14. K. Erickson, R. D. Braun, D. Yu, J. Lanzen, D. Wilson, D. M. Brizel, T. W. Secomb, J. E. Biaglow, and M. W. Dewhirst, *Cancer Res.*, **63**, 4705 (2003).
15. K. E. Garrison, S. A. Pasas, J. D. Cooper, and M. I. Davies, *Eur. J. Pharm. Sci.*, **17**, 1 (2002).
16. M. Muller, *Adv. Drug Delivery Rev.*, **45**, 255 (2000).
17. K. A. Salem, A. Szymanski-Exner, R. S. Lazebnik, M. S. Breen, J. Gao, and D. L. Wilson, *IEEE Trans. Med. Imaging*, **21**, 1310 (2002).
18. A. Szymanski-Exner, N. T. Stowe, K. Salem, R. Lazebnik, J. R. Haaga, D. L. Wilson, and J. Gao, *J. Pharm. Sci.*, **92**, 289 (2003).
19. W. Wolf, *Adv. Drug Delivery Rev.*, **41**, 1 (2000).
20. R. E. Port and W. Wolf, *Invest. New Drugs*, **21**, 157 (2003).
21. A. J. Fischman, N. M. Alpert, and R. H. Rubin, *Clin. Pharmacokinet.*, **41**, 581 (2002).
22. B. J. Gudzinowicz, B. T. Younkin, Jr., and M. J. Gudzinowicz, *Drug Dynamics for Analytical, Clinical, and Biological Chemists*, Marcel Dekker, New York (1984).
23. X. Li and W. K. Chan, *Adv. Drug Deliv. Rev.*, **39**, 81 (1999).
24. V. T. DeVita, C. Denham, J. D. Davidson, and V. T. Oliverio, *Clin. Pharmacol. Ther.*, **8**, 566 (1967).
25. J. T. Santini, Jr., M. J. Cima, and R. Langer, *Nature (London)*, **397**, 335 (1999).
26. G. Voskerician, M. S. Shive, R. S. Shawgo, H. von Recum, J. M. Anderson, M. J. Cima, and R. Langer, *Biomaterials*, **24**, 1959 (2003).
27. G. J. Burger, E. J. T. Smulders, J. W. Berenschot, T. S. J. Lammerink, J. H. J. Fluitman, and S. Imai, *Sens. Actuators, A*, **54**, 669 (1996).
28. Y. C. Wu and W. F. Koch, *J. Solution Chem.*, **20**, 391 (1991).
29. P. Atkins, *Physical Chemistry*, p. 834, W. H. Freeman & Co., New York (1994).
30. P. Vaný́sek, in *CRC Handbook of Chemistry and Physics*, 73rd ed., D. R. Lide, Chief Editor, pp. 5-110, CRC Press, Boca Raton, FL (1992).
31. A. J. Bard and L. R. Faulkner, *Electrochemical Methods*, p. 376, Wiley, New York (1980).
32. Z. Lukacs, *J. Electroanal. Chem.*, **432**, 79 (1997).
33. A. Van Hook, *Crystallization Theory and Practice*, p. 130, Reinhold, New York (1961).
34. J. Christoffersen and M. R. Christoffersen, in *The Experimental Determination of Solubilities*, G. T. Hefter and R. P. T. Tomkins, Editors, p. 77, Wiley, New York (2003).
35. W. M. Deen, *Analysis of Transport Phenomena*, p. 91, Oxford University Press, New York (1998).